JVST A
Journal of Vacuum Science & Technology A

Epitaxial growth of the first two members of the $Ba_{n+1}In_nO_{2.5n+1}$ Ruddlesden–Popper homologous series

Cite as: J. Vac. Sci. Technol. A **40**, 062707 (2022); https://doi.org/10.1116/6.0002205
Submitted: 07 September 2022 • Accepted: 18 October 2022 • Published Online: 14 November 2022

Felix V. E. Hensling, Michelle A. Smeaton, Veronica Show, et al.

COLLECTIONS

Paper published as part of the special topic on Thin Film Deposition for Materials Discovery

This paper was selected as Featured

JVST A
Journal of Vacuum Science & Technology A

ARTICLE

avs.scitation.org/journal/jva

Epitaxial growth of the first two members of the $Ba_{n+1}In_nO_{2.5n+1}$ Ruddlesden–Popper homologous series

Cite as: J. Vac. Sci. Technol. A 40, 062707 (2022); doi: 10.1116/6.0002205
Submitted: 7 September 2022 · Accepted: 18 October 2022 ·
Published Online: 14 November 2022

Felix V. E. Hensling,[1,a)] Michelle A. Smeaton,[1] Veronica Show,[2] Kathy Azizie,[1] Matthew R. Barone,[1,2] Lena F. Kourkoutis,[3,4] and Darrell G. Schlom[1,4,5]

AFFILIATIONS

[1]Department of Materials Science and Engineering, Cornell University, Ithaca, New York 14853
[2]Platform for the Accelerated Realization, Analysis, and Discovery of Interface Materials (PARADIM), Cornell University, Ithaca, New York 14853
[3]School of Applied and Engineering Physics, Cornell University, Ithaca, New York 14853
[4]Kavli Institute at Cornell for Nanoscale Science, Ithaca, New York 14853
[5]Leibniz-Institut für Kristallzüchtung, Max-Born-Strasse 2, 12849 Berlin, Germany

Note: This paper is a part of the Special Topic Collection on Thin Film Deposition for Materials Discovery.
[a)]**Electronic mail:** hensling@cornell.edu

ABSTRACT

We demonstrate the epitaxial growth of the first two members, and the $n = \infty$ member of the homologous Ruddlesden–Popper series of $Ba_{n+1}In_nO_{2.5n+1}$ of which the $n = 1$ member was previously unknown. The films were grown by suboxide molecular-beam epitaxy where the indium is provided by a molecular beam of indium-suboxide [In_2O (g)]. To facilitate *ex situ* characterization of the highly hygroscopic barium indate films, a capping layer of amorphous SiO_2 was deposited prior to air exposure. The structural quality of the films was assessed by x-ray diffraction, reflective high-energy electron diffraction, and scanning transmission electron microscopy.

Oxide Ruddlesden–Popper (RP) phases describe the homologous series of the perovskite-related $A_{n+1}B_nO_{3n+1}$ phases, where n represents the number of perovskite unit cells sandwiched between double rock salt layers as illustrated in Fig. 1.[1–3] The interest in RP phases is based on the intriguing and often fundamentally different physical properties that the distinct members of the series exhibit. A famous example is the $Sr_{n+1}Ru_nO_{3n+1}$ series where with an increase of n, the phase changes from superconducting ($n = 1$)[4] to ferromagnetic ($n = 3$–5).[5] Consequently RP phases are highly pertinent to a wide variety of applications, e.g., tunable dielectrics,[6,7] resistive switching,[8] and photovoltaics.[9,10]

The trend toward the formation energy of phase n being degenerate with phase $n + 1$ (or $n - 1$) and an increasingly close cation stoichiometry with an increasing n make RP phases challenging to synthesize by most methods, especially for large n. Molecular-beam epitaxy (MBE) with its unique flux control paired with recent developments in an improved *in situ* growth control of RP phases can, however, overcome these challenges.[11,54]

The $Ba_{n+1}In_nO_{2.5n+1}$ homologous RP series differs from most RP series as the perovskite end member $BaInO_{2.5}$ usually referred to as $n = \infty$ contains a huge concentration of oxygen vacancies. If these oxygen vacancies arrange in an ordered rather than a random manner, the $n = \infty$ member transforms into the brownmillerite $Ba_2In_2O_5$. The literature is equivocal over the parameters promoting this transformation.[12–14] In addition to the $n = \infty$ phase, two other members of the $Ba_{n+1}In_nO_{2.5n+1}$ homologous RP series have been synthesized in bulk: $n = 2$[15] and $n = 3$.[16] The lack of evidence in the literature for an $n = 1$ phase is a result of another phase forming for the same cation ratio, $Ba_4In_2O_7$ with a unique structure sometimes misidentified as $Ba_5In_2O_8$, not related to the RP series.[17–20]

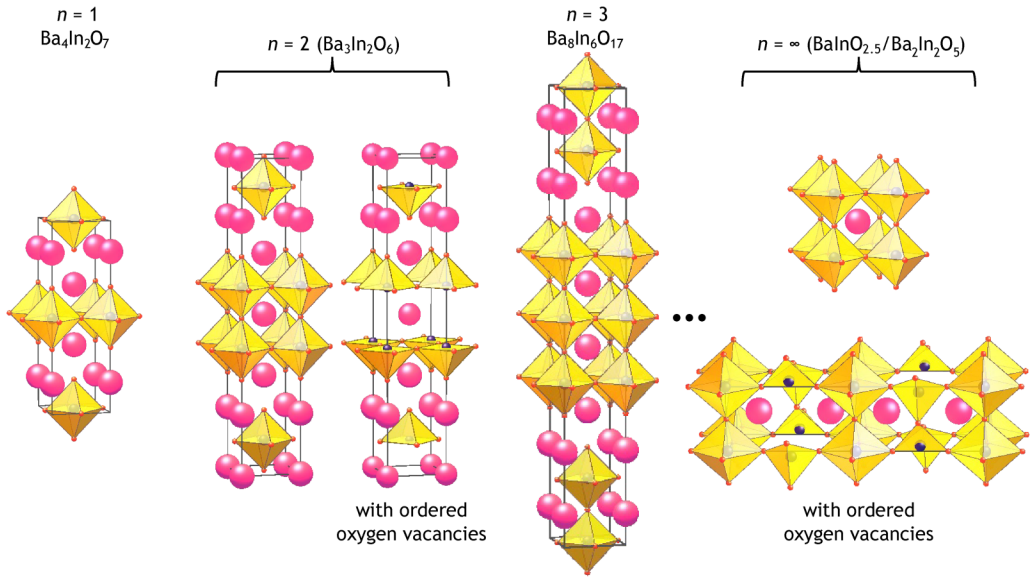

FIG. 1. General structure of the homologous $A_{n+1}B_nO_{3n+1}$ RP phases with increasing n from left to right. The oxygen octahedra around the violet *B*-site atoms are depicted in yellow, the *A*-site atoms in magenta, and the oxygen atoms in red. The specific structures of the $Ba_{n+1}In_nO_{2.5n+1}$ series with oxygen vacancy ordering are included for the structures where the oxygen vacancy order is known, namely, the observed oxygen vacancy order for the $n = 2$ and $n = \infty$ phase. For clarity, only a quarter of the ordered $n = \infty$ unit cell is depicted.

Intriguing properties for the known members of the $Ba_{n+1}In_nO_{2.5n+1}$ homologous RP series are either predicted or already known. The $n = \infty$ perovskite $BaInO_{2.5}$ and brownmillerite $Ba_2In_2O_5$ both combine high proton and oxygen conductivity and are, thus, interesting for applications such as solid oxide fuel cells.[21–23] When it was first prepared as a high-quality single crystal, $Ba_3In_2O_6$ was considered a potential high transition temperature (T_c) superconductor based on its structure which is closely related to the $n = 2$ RP phase $Sr_3Ti_2O_7$ and isostructural to the known high-T_c superconductors $La_{(2-x)}Sr_xCaCu_2O_6$ and $La_2CaCu_2O_{(6+\delta)}$.[15,24,25] More recently, machine learning efforts to map out potential high T_c superconductors have predicted it to have a T_c of 45.9 K.[26] Despite this to our knowledge, there are no reports of the epitaxial growth of any members of the $Ba_{n+1}In_nO_{2.5n+1}$ homologous RP series. A possible reason for this is the rather challenging growth. The large *a*-axis bulk lattice constants of the known members of the $Ba_{n+1}In_nO_{2.5n+1}$ homologous RP series ($Ba_3In_2O_6$ $a = 0.419$ nm,[27] $Ba_8In_6O_{17}$ $a = 0.417$ nm)[16] suggest a limited choice of substrates and most barium-containing indates are highly hygroscopic.[20] The hygroscopy of $Ba_3In_2O_6$ is also the reason why its potential superconductivity was not investigated for single crystals.[15]

In this letter, we describe the growth and structural characterization of the first two members of the $Ba_{n+1}In_nO_{2.5n+1}$ homologous RP series by MBE of which the $n = 1$ member was previously unknown. The films were grown using a molecular beam of In_2O emanating from a suboxide source; such growth is referred to as suboxide molecular-beam epitaxy (S-MBE). S-MBE has previously been demonstrated as a powerful tool for the growth of III–VI materials at high growth rates and low substrate temperature with high structural perfection.[28–30] This S-MBE approach for the growth of $Ba_{n+1}In_nO_{2.5n+1}$ phases produces films with high crystalline quality as revealed by x-ray diffraction (XRD) and scanning transmission electron microscopy (STEM). The successful growth of RP phases by codeposition proves the applicability of S-MBE for a system requiring precise flux calibrations. The stability of the hygroscopic films is substantially increased by an *in situ* deposited layer of amorphous SiO_2. We see indications for the formation of both $n = \infty$ members (the perovskite and the brownmillerite member) being dependent on the choice of substrate.

All films are grown in a Veeco Gen10 MBE. The growth temperature is measured by an optical pyrometer at a measurement wavelength of 980 nm. A substrate temperature of 950 °C is employed as lower temperatures promote the formation of undesired compounds according to the Ba–In–O phase diagram.[14] The barium-containing indate films are grown in a mixture of approximately 10% distilled ozone and 90% oxygen at a background pressure of 10^{-6} Torr. Before the deposition of the amorphous SiO_2 capping layer, the substrate is cooled to ≤ 350 °C and the oxidant background pressure is decreased to 5×10^{-7} Torr. The growth is monitored in real time by reflection high-energy electron diffraction (RHEED). Barium is evaporated from an elemental source. The In_2O (g) suboxide molecular beam is obtained from heating a mixture of indium and In_2O_3 powders with a mole fraction of oxygen $x(O) = 0.4$ (provided by the In_2O_3 powder) in a SUMO medium-temperature MBE effusion cell (Sumo® is a registered trademark of Veeco Instruments, Inc.). An indium + In_2O_3 mixture with $x(O) = 0.4$ has proven to give the most stable and pure

In_2O flux,[30] note that a gallium + Ga_2O_3 mixture with $x(O) = 0.4$ is used to produce a Ga_2O (g) suboxide molecular beam in the growth of Ga_2O_3 films by S-MBE.[28,29] The silicon species for the SiO_2 capping is supplied by a molecular beam of SiO (g) emanating from a standard medium-temperature MBE source containing chunks of amorphous SiO.[31–33] The fluxes of barium and In_2O are roughly established by a quartz-crystal microbalance (QCM) and refined by the subsequent growth of binary oxide calibration films.[34] The thickness of the amorphous SiO_2 capping layer is calibrated by growing an amorphous SiO_2 film directly on a (001) MgO substrate and subsequently measuring the thickness by x-ray reflectivity (XRR) obtained with a Panalytical Empyrean with Cu-$K_{\alpha 1}$ radiation. (001) MgO substrates are supplied by CrysTec GmbH, and (001) $SrTiO_3$ substrates are supplied by Shinkosha Co. Ltd and prepared as described by Koster *et al.*[35,36]

Cross-sectional STEM specimens were prepared using a Thermo Fisher Scientific Helios G4 UX focused ion beam (FIB) using standard lift out and thinning methods. HAADF-STEM data were acquired using a Thermo Fisher Scientific Spectra 300 X-CFEG operating at 300 kV with a convergence angle of 21.4 mrad. Inner and outer collection angles were approximately 60 and 200 mrad, respectively. To obtain high signal-to-noise-ratio (SNR), many image frames were acquired at fast acquisition rates and then aligned using a rigid registration process optimized for noisy images.[37] STEM specimens were stored in a vacuum chamber between FIB preparation and imaging to minimize air exposure.

For any homologous RP series, the $n = 1$ member has the highest A/B ratio ($A/B = 2$ for $n = 1$) and as n increases A/B approaches one. Once it reaches $A/B = 1$, it is called the $n = \infty$ member which is usually a perovskite, but in the case of $Ba_{n+1}In_nO_{2.5n+1}$ can also be a brownmillerite if the oxygen vacancies order into planes. An approach for achieving the different members of a homologous RP series in codeposition is to start with an A/B ratio of two and to subsequently decrease the ratio systematically. Considering the aforementioned large a-axis lattice constant of all known members of the $Ba_{n+1}In_nO_{2.5n+1}$ RP series, we choose (001) MgO as a substrate. In addition to its large a-axis lattice constant (0.42 nm),[39] it has the advantage of industrial relevance.[40–44] Its obvious drawback is the nonperovskite structure. All discussed films have a thickness of ≈ 160 nm.

Following the strategy of starting with Ba/In = 2, the resulting film under the aforementioned conditions shows the green diffraction pattern shown in Fig. 2(a). The pattern is indicative of a phase-pure film. The peak positions do not, however, correspond to the non-RP phase previously reported for this cation ratio[19] and correspond to a c-lattice constant of 1.34 nm. If we compare this pattern to the diffraction pattern of epitaxial $n = 1$ RP phases, e.g., Sr_2TiO_4[45] and Sr_2RuO_4,[5] a strong resemblance is noticeable. This is the first hint of the successful growth of the previously unknown $n = 1$ member, $Ba_4In_2O_7$, of the $Ba_{n+1}In_nO_{2.5n+1}$ RP series. This hypothesis is further substantiated by the RHEED image along the [100] in-plane axis of the film in Fig. 2(b). It shows the typical pattern for the expected in-plane perovskite-related structure and is sharp with slightly visible Kikuchi lines, indicating a smooth surface and high surface crystallinity. The bulk crystallinity is equally of high quality as evident from the full width half maximum (FWHM) of the rocking

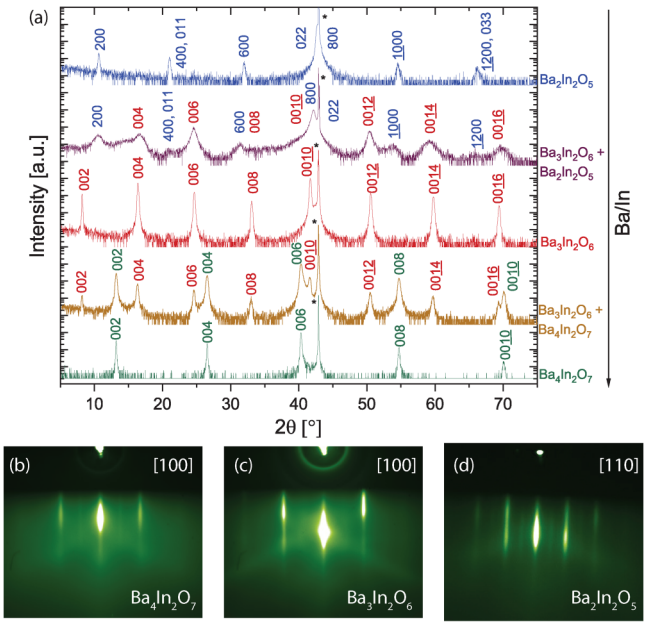

FIG. 2. (a) θ–2θ XRD scans of epitaxial films with varying Ba/In content offset along the y-axis for clarity. All films are about 160 nm thick and are grown on (001) MgO substrates. The 002 MgO substrate peaks are marked by an asterisk (*). Cation ratios not fitting an exact phase stoichiometry result in a phase mixture (brown and purple). The diffraction pattern shown in green best agrees with the c-axis of the previously unknown $n = 1$ RP phase $Ba_4In_2O_7$ and we indexed it accordingly. The red diffraction pattern exhibits sharp peaks of high intensity at positions expected for c-axis oriented $Ba_3In_2O_6$ based on its bulk lattice constant as reported by Antipov *et al.* (Ref. 27). The blue diffraction pattern is in agreement with epitaxial (100)-oriented brownmillerite $Ba_2In_2O_5$ based on the bulk lattice constant. The peak positions expected for an (011)-oriented brownmillerite as reported by Fischer *et al.* are also marked behind the comma (Ref. 38). RHEED patterns taken during growth along the [100] azimuth of the 160 nm thick epitaxial films of (b) $Ba_4In_2O_7$ and (c) $Ba_3In_2O_6$. The Kikuchi lines and sharp features are a sign of the good crystal and surface quality. (d) RHEED pattern along the [110] azimuth of a 160 nm thick film of $Ba_2In_2O_5$.

curve of the 006 peak of this phase being dominated by the substrate quality: 0.03° (see Fig. S1 in the supplementary material).[53]

As per our strategy in the next step, we increase the In_2O flux and, thus, decrease the Ba/In-ratio. For the resulting film, we observe the brown diffraction pattern in Fig. 2(a). It shows a mix of $Ba_4In_2O_7$ and a second phase. This second phase is easily identified considering the diffraction pattern resulting for a further increased Ba/In-ratio of 3/2 (red). At a Ba/In ratio of 3/2, the θ–2θ scan in XRD displays phase-pure narrow peaks of exceptional intensity in agreement with the bulk c-axis lattice constant of $Ba_3In_2O_6$.[27] The RHEED pattern along the [100] azimuth of the $Ba_3In_2O_6$ film shows defined streaks and clear Kikuchi lines, again indicating a smooth surface and high surface crystallinity [Fig. 2(c)]. The narrow FWHM of the rocking curve of the $00\underline{10}$ peak of the $Ba_3In_2O_6$ film (0.11°, see Fig. S1 in the supplementary material[53]) indicates high crystalline quality, however, less so than the $n = 1$ film. A possible reason is a

rotation of adjacent perovskite layers with respect to each other as shown in Fig. S2 (a) in the supplementary material.[53]

An even further decrease of the Ba/In-ratio again results in a film with a diffraction pattern [purple Fig. 2(a)] indicative of a mixture of phases. It shows broadened peaks at the same positions as the $Ba_3In_2O_6$ film (red) plus additional peaks. These peaks are at the same positions as the peaks of the diffraction pattern for the film grown with a Ba/In-ratio of 1:1 [blue Fig. 2(a)] and are in agreement with the bulk *a*-lattice constant of the brownmillerite $Ba_2In_2O_5$ (space group *Ima*2; $a = 1.672$ nm, $b = 0.608$ nm, $c = 0.596$ nm).[38] For growth on (001) MgO, the diffraction pattern, thus, suggests the epitaxial growth of a (100)-oriented brownmillerite $Ba_2In_2O_5$ film.

The phase observed is different when this same 1:1 flux ratio of Ba/In is incident on a (001) $SrTiO_3$ substrate. Figure 3 shows the diffraction for a film grown with a Ba/In-ratio of 1:1 (light blue) on a (001) $SrTiO_3$ substrate. The diffraction pattern does not show the peaks expected for the (100) brownmillerite phase. Instead peaks and peak intensity ratios in agreement with the bulk *c*-lattice constant of the perovskite $BaInO_{2.5}$ are seen.[12] The difference is also obvious from the RHEED images of both $n = \infty$ films. The epitaxial brownmillerite grown on (001) MgO shows pronounced additional reflections at the half-order position of the substrate [Fig. 2(d)] suggesting a doubled unit cell. The epitaxial perovskite phase of $BaInO_{2.5}$ grown on (001) $SrTiO_3$ exhibits the RHEED pattern shown in the inset of Fig. 3, which is typical for a perovskite and shows no reflections at the half-order position of the substrate (see Fig. S3 in the supplementary material[53]). An explanation for this substrate-dependent observation of two different phase-pure $n = \infty$ films is that at the given growth parameters the formation of the brownmillerite phase is energetically favorable; the perovskite structure of the $SrTiO_3$ substrate, however, epitaxially stabilizes[46–50] the perovskite phase. We cannot completely exclude the formation of (011)-oriented brownmillerite formation on (001) $SrTiO_3$ as its peaks coincide with the perovskite peaks indicated in Fig. 3. Nonetheless, the RHEED pattern and peak intensity ratios of the diffraction pattern suggest a perovskite film.

The red diffraction pattern in Fig. 3 belongs to the $n = 2$ RP phase grown on (001) $SrTiO_3$. The diffraction pattern of the $n = 2$ $Ba_3In_2O_6$ film is, despite the much higher lattice mismatch on (001) $SrTiO_3$ of 7.4% compared with −0.7% on (001) MgO, of similar structural quality. The much higher FWHM of the rocking curve (0.48°, see Fig. S1 in the supplementary material[53]), despite the isostructural substrate, means that the increased mismatch has a stronger negative effect on the crystalline quality than the isostructural substrate has a positive effect.

Comparing our x-ray diffraction data to the general structures in Fig. 1, we are able to epitaxially synthesize the $n = \infty$ members, the $n = 2$ member, $Ba_3In_2O_6$, and the previously unknown $n = 1$ member, $Ba_4In_2O_7$. As an additional check of our proposed structure for $Ba_4In_2O_7$ (shown in Fig. 1), we compare a simulated diffraction pattern of it to the measured diffraction pattern from Fig. 2(a) in Fig. 4. We find good agreement between the measured and calculated diffraction patterns. This strengthens our claim of having grown the previously unknown $n = 1$ RP phase, $Ba_4In_2O_7$.

While the x-ray diffraction data suggest we are able to grow high-quality, phase-pure epitaxial films of the first two members of the $Ba_{n+1}In_nO_{2.5n+1}$ homologous RP series, we have further assessed the crystalline structure and quality by STEM. Figure 5 shows cross-sectional HAADF-STEM images of the films and corroborates the identities of the phases hypothesized above. The $n = 1$ and the $n = 2$ RP phases are shown in Figs. 5(a) and 5(b), respectively, and the $Ba_2In_2O_5$ brownmillerite phase is shown in Figs. 5(c) and 5(d). The depicted images are representative off all observed sample areas. Figure 5(a) confirms that we have indeed

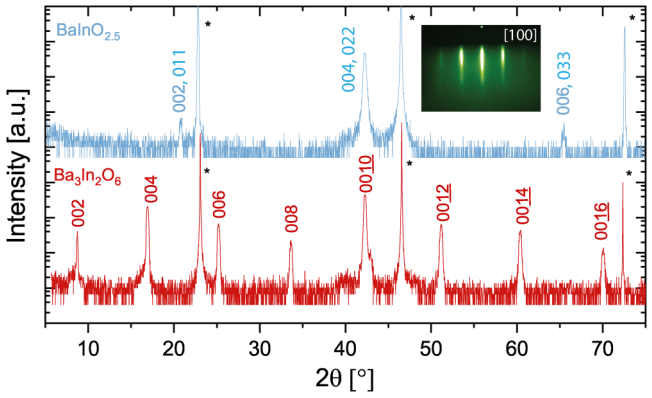

FIG. 3. θ–2θ scans of a 160 nm thick $Ba_3In_2O_6$ film (red) and a 160 nm thick perovskite $BaInO_{2.5}$ film (light blue) grown on (001) $SrTiO_3$ with the film peaks indexed accordingly. The peak positions expected for an (011)-oriented brownmillerite are also marked following the comma (Ref. 38). The peaks marked by asterisks (*) are the $SrTiO_3$ substrate peaks. The diffraction peaks are in good agreement with the respective values expected from the bulk *c*-lattice constants reported previously (Refs. 12 and 27). The inset shows the RHEED pattern along the [100] azimuth of the $BaInO_{2.5}$ film at the end of the growth.

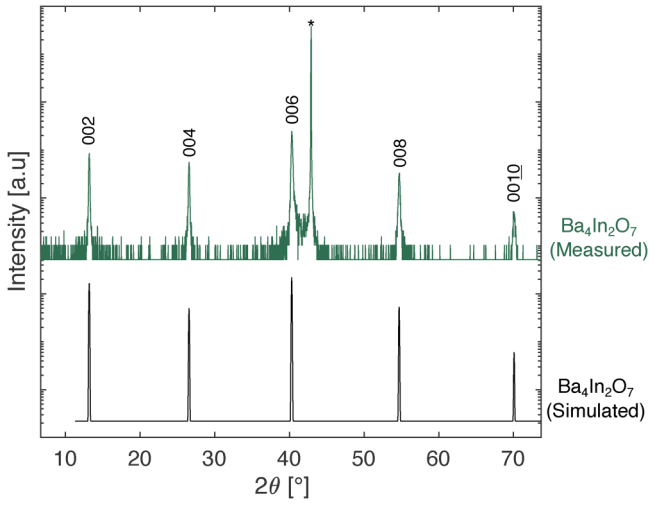

FIG. 4. Comparison of a simulated θ–2θ scan for the proposed $Ba_4In_2O_7$ structure to the measured θ–2θ scan from Fig. 2(a).

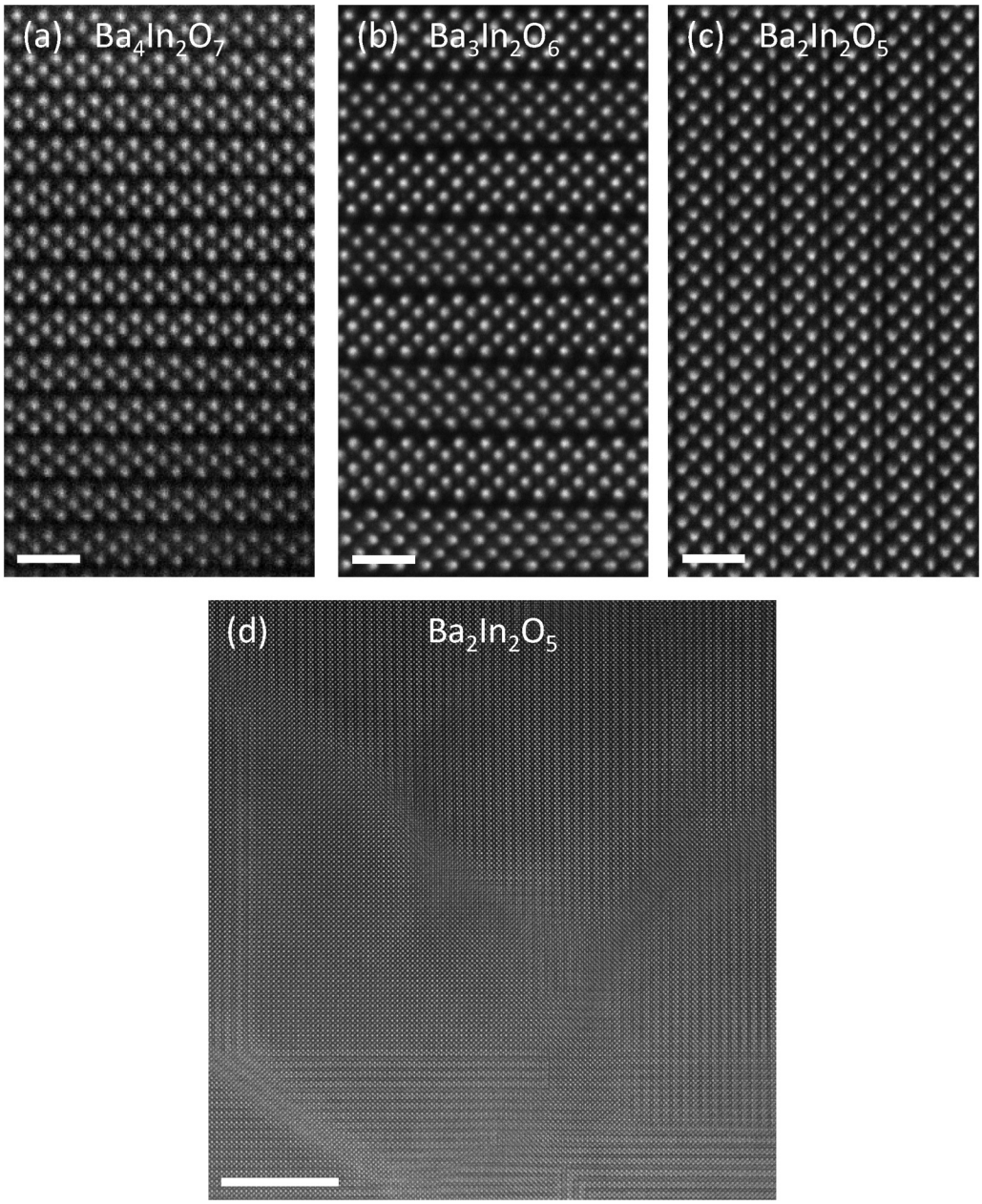

FIG. 5. Cross-sectional HAADF-STEM images of (a) $n = 1$ $Ba_4In_2O_7$, (b) $n = 2$ $Ba_3In_2O_6$, (c) the brownmillerite $Ba_2In_2O_5$, and (d) an overview scan of the brownmillerite $Ba_2In_2O_5$. The expected ordering for the respective $n = 1$ and $n = 2$ RP phases is clearly visible with the dark lines indicative of the double rock salt BaO layers. The brownmillerite in (c) is (011)-oriented. (d) reveals that the (011) and the (100) orientation coexist throughout the film. Scale bars for (a)–(c) are 1 nm. Scale bar for (d) is 10 nm.

epitaxially grown the previously unknown $n = 1$ RP phase, $Ba_4In_2O_7$. Figure 5(b) verifies the high quality of the epitaxial $Ba_3In_2O_6$ film grown on (001) MgO with the expected oxygen vacancy ordering. Nonetheless, some defects can be found within the $Ba_3In_2O_6$ film and are discussed in Fig. S2 in the supplementary material.[53] Most interestingly, an on- and off-axis rotation of adjacent perovskite layers is commonly observed throughout the film which, as evident by the diffraction data shown in Fig. 4(a), has no effect on the *c*-lattice constant. Figure 5(c) reveals a (011) orientation of the epitaxial brownmillerite which is

in agreement with the RHEED image in Fig. 2(d), but not expected from the θ–2θ scan in Fig. 2(a). The broader overview HAADF-STEM image in Fig. 5(d) reveals that both orientations (011) and (100) coexist throughout the film. Some areas also show a contrast consistent with either the perovskite phase or a projection through stacking faults of the (100)- and/or (011)-oriented brownmillerite phase; latter being more likely considering the θ–2θ scan in Fig. 2(a). The lack of a (011) related diffraction pattern in Fig. 2(a) is easily explained by the peak positions. The 011 peak is hidden by the 400 peak of the (100)-oriented brownmillerite and the 022 peak is at the same position as the 002 substrate peak.

At this point, we can comfortably claim the ability to grow the first two members of the $Ba_{n+1}In_nO_{2.5n+1}$ RP homologous series as well as the $n = \infty$ members. We overcame the general challenge of RP phases needing precise stoichiometry control and did so utilizing an indium suboxide source, demonstrating its applicability to the growth of these layered indates. We overcame the specific challenge of the large a-axis lattice parameters of the barium-containing indates by using (001) MgO substrates, but our results suggest that $Ba_{n+1}In_nO_{2.5n+1}$ phases even grow epitaxially on highly mismatched substrates such as (001) $SrTiO_3$. The remaining challenge to the growth of barium-containing indates is hygroscopy.

All of the films discussed thus far were capped with a 50 nm thick amorphous SiO_2 layer. The importance of this capping layer will be discussed for the specific example of $Ba_3In_2O_6$ films grown on (001) MgO. Figure 6(a) shows θ–2θ scans of two stoichiometric 160 nm thick $Ba_3In_2O_6$ films. One of them was not capped. It was exposed to air and measured by XRD (blue). The other was capped with 50 nm of amorphous SiO_2 before exposing it to air for the XRD measurement (red). The capped film is the same film as shown in Fig. 2(a). Both films were measured immediately after growth (bottom), after five days of storage in a desiccator (center), and for the capped sample after 45 days of storage in a desiccator (top). The θ–2θ scans of the uncapped and capped films are offset along the y-axis for clarity. It is obvious that the uncapped sample, despite storage in a desiccator, is not stable. The only peak remaining after five days is the 002 peak of the MgO substrate. In stark contrast to this behavior, all film peaks of the capped film remain after five days. Only the formation of a shoulder on the lower 2θ angle side of the lower-angle 00ℓ peaks (up to $00\underline{10}$) is observed. After 45 days, there is slightly more change. Instead of shoulders additional broad peaks can be observed at the former shoulder positions. These broad peaks coincide with the barium-poor phases discussed above, making a loss of barium by hydroxylation probable. The observation at lower diffraction angles which are more surface sensitive means that the hydroxylation likely happens at the surface. Nonetheless, the distinct $Ba_3In_2O_6$ diffraction pattern stays intact. A scan of the $00\underline{10}$ peak over a narrow θ–2θ range that includes the 002 MgO substrate peak [Fig. 6(b)] reveals that even the thickness fringes are still visible after 45 days of storage, a sign of preserved good crystallinity and a smooth surface.

Figure 6(c) shows a cross-sectional HAADF-STEM image of a similar capped sample with a 50 nm thick amorphous SiO_2 layer after being stored for over 120 days in a desiccator. The typical 1/5 ordering of $n = 2$ RP phases is maintained, which further demonstrates the preservation of the crystal quality of the sample by capping.

Prolonging the stability of epitaxial barium-containing indate films in general, and $Ba_3In_2O_6$, in particular, enables their properties to be investigated. The electrical properties of $Ba_3In_2O_6$ will be reported elsewhere.[51] It will also enable the investigation of the previously unknown $n = 1$ RP member $Ba_4In_2O_7$, which we demonstrated in this paper for the first time. We expect that higher-n members of the $Ba_{n+1}In_nO_{2.5n+1}$ RP homologous series, e.g., the

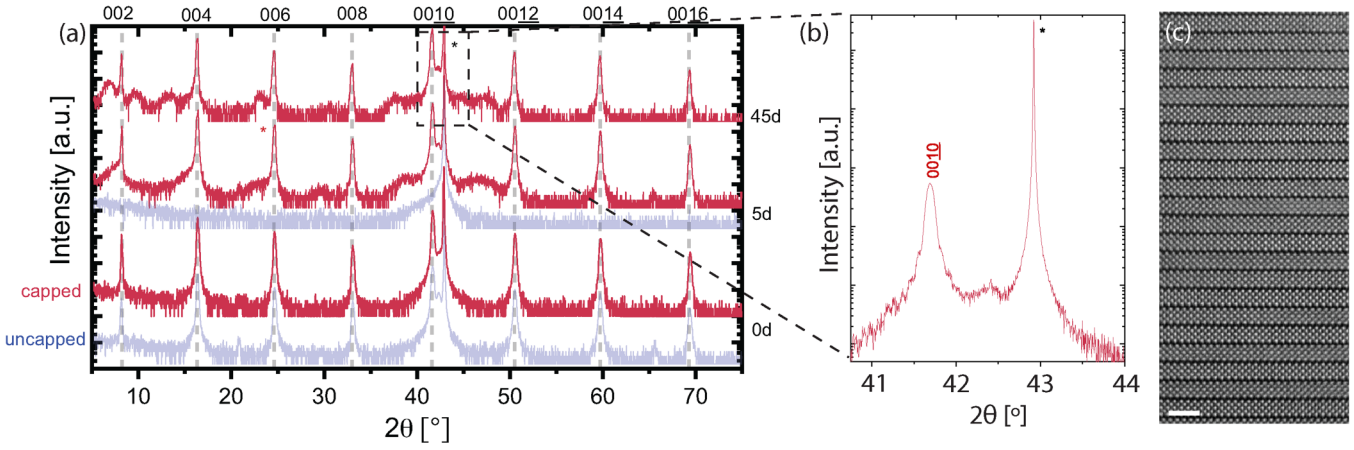

FIG. 6. (a) θ–2θ scans of an uncapped (blue) and a capped (red) $Ba_3In_2O_6$ film as a function of time after air exposure. Both films were stoichiometric as grown and ≈ 160 nm thick. The scans are offset along the y-axis for clarity. For the uncapped film, complete loss of crystallinity (no peaks remain) is seen after five days of being stored in a desiccator (center). For the capped film, the crystalline structure remains mostly intact for 45 days (top). This is further indicated by the thickness fringes of the $00\underline{10}$ film peak remaining visible after 45 days (b). (c) Representative HAADF-STEM image showing the characteristic 1/5 ordering of an n=2 RP phase even after an $\overline{SiO_2}$ capped film is stored for over 120 days in a desiccator. Scale bar is 2 nm.

$n = 3$ member, $Ba_8In_6O_{17}$, that has already been demonstrated in bulk,[16] or yet to be demonstrated higher n can be grown by changing from codeposition to more advanced shuttered growth strategies.[11,54] Our ability to grow the $n = 1$ and $n = 2$ members by codeposition with high crystalline quality demonstrates the applicability of the newly developed In_2O suboxide source to growths requiring a precise flux calibration.

The potential ability to select between the formation of the $n = \infty$ phases of perovskite $BaInO_{2.5}$ and brownmillerite $Ba_2In_2O_5$ is of interest for the solid oxide fuel cell community as mentioned in the Introduction. Epitaxial films have recently been investigated by this community as model materials as they allow the influence of film microstructure, crystal orientation, strain, and other factors on the material's performance to be investigated.[52]

ACKNOWLEDGMENTS

F.V.E.H., M.A.S., V.S., K.A., M.B., L.F.K., and D.G.S. acknowledge support from the National Science Foundation [Platform for the Accelerated Realization, Analysis, and Discovery of Interface Materials (PARADIM)] under Cooperative Agreement No. DMR-2039380. Substrate preparation was performed in part at the Cornell NanoScale Facility, a member of the National Nanotechnology Coordinated Infrastructure (NNCI), which is supported by the National Science Foundation (Grant No. NNCI-2025233). This work made use of the Cornell Center for Materials Research Shared Facilities, which are supported through the NSF MRSEC program (DMR-1719875). M.A.S. acknowledges additional support from the NSF GRFP under Award No. DGE-2139899. This research was funded in part by the Gordon and Betty Moore Foundation's EPiQS Initiative through Grant No. GBMF9073 to Cornell University.

F.V.E.H. acknowledges funding by the Alexander von Humboldt foundation in the form of a Feodor Lynen fellowship. The authors acknowledge Sean Palmer for substrate preparation and technical support.

AUTHOR DECLARATIONS

Conflict of Interest

The authors have no conflicts to disclose.

Author Contributions

Felix V. E. Hensling: Conceptualization (lead); Data curation (lead); Formal analysis (lead); Funding acquisition (supporting); Investigation (lead); Methodology (equal); Writing – original draft (lead); Writing – review & editing (equal). **Michelle A. Smeaton:** Data curation (equal); Formal analysis (equal); Investigation (equal); Methodology (equal); Writing – original draft (supporting); Writing – review & editing (equal). **Veronica Show:** Data curation (supporting); Formal analysis (supporting); Visualization (supporting); Writing – review & editing (supporting). **Kathy Azizie:** Data curation (supporting); Methodology (supporting). **Matthew R. Barone:** Data curation (equal); Formal analysis (equal); Investigation (equal); Methodology (equal); Writing – original draft (supporting); Writing – review & editing (equal). **Lena F. Kourkoutis:** Funding acquisition (equal); Project administration (equal); Supervision (equal); Writing – review & editing (equal). **Darrell G. Schlom:** Conceptualization (equal); Funding acquisition (lead); Project administration (lead); Supervision (lead); Writing – review & editing (lead).

DATA AVAILABILITY

The data supporting the findings of this study are available within the paper. Additional data related to the growth and structural characterization are available in the PARADIM data repository at https://doi.org/10.34863/e7qx-7487, Ref. 55. Any additional data connected to the study are available from the corresponding author upon reasonable request.

REFERENCES

[1]D. Balz and K. Plieth, Z. Elektrochem. Ber. Bunsen. Phys. Chem. **59**, 545 (1955).
[2]S. N. Ruddlesden and P. Popper, Acta Crystallogr. **10**, 538 (1957).
[3]S. N. Ruddlesden and P. Popper, Acta Crystallogr. **11**, 54 (1958).
[4]Y. Maeno, H. Hashimoto, K. Yoshida, S. Nishizaki, T. Fujita, J. G. Bednorz, and F. Lichtenberg, Nature **372**, 532 (1994).
[5]W. Tian *et al.*, Appl. Phys. Lett. **90**, 022507 (2007).
[6]C. H. Lee *et al.*, Nature **502**, 532 (2013).
[7]N. M. Dawley *et al.*, Nat. Mater. **19**, 176 (2020).
[8]K. Shibuya, R. Dittmann, S. Mi, and R. Waser, Adv. Mater. **22**, 411 (2010).
[9]B. Kressdorf *et al.*, Phys. Rev. Appl. **14**, 1 (2020).
[10]H. Tsai *et al.*, Nature **536**, 312 (2016).
[11]M. R. Barone *et al.*, APL Mater. **9**, 021118 (2021).
[12]K. Mader and H. Müller-Buschbaum, Z. Anorg. Allg. Chem. **528**, 125 (1985).
[13]D. Gregory and M. Weller, J. Solid State Chem. **107**, 134 (1992).
[14]R. Horyń, E. Bukowska, and A. Sikora, J. Alloys Compd. **305**, 103 (2000).
[15]K. Mader and H. Müller-Buschbaum, Z. Anorg. Allg. Chem. **559**, 89 (1988).
[16]K. Mader and H. Müller-Buschbaum, J. Less Common Met. **157**, 71 (1990).
[17]T. Kalinina, L. Lykova, L. Kovba, M. Melnikova, and N. Porotnikov, Zh. Neorg. Khim. **28**, 466 (1983).
[18]P. Villars, K. Cenzual, J. Daams, R. Gladyshevskii, O. Shcherban, V. Dubenskyy, V. Kuprysyuk, I. Savysyuk, and R. Zaremba, "$Ba_4In_2O_7$," in *Landolt-Börnstein—Group III Condensed Matter 43A10* (Springer-Verlag, Berlin Heidelberg, 2011), Vol. 56, pp. 374–374.
[19]A. Lalla and H. Mueller-Buschbaum, Z. Anorg. Allg. Chem. **573**, 12 (1989).
[20]W. Kwestroo, H. van Gerven, and C. Langereis, Mater. Res. Bull. **12**, 157 (1977).
[21]G. B. Zhang and D. M. Smyth, Solid State Ionics **82**, 153 (1995).
[22]G. B. Zhang and D. M. Smyth, Solid State Ionics **82**, 161 (1995).
[23]N. Hideshima and K. Hashizume, Solid State Ionics **181**, 1659 (2010).
[24]R. J. Cava *et al.*, Nature **345**, 602 (1990).
[25]I. Tsukada, Y. Nagao, and Y. Ando, Phys. Rev. B **69**, 1 (2004).
[26]Z.-L. Liu, P. Kang, Y. Zhu, L. Liu, and H. Guo, APL Mater. **8**, 061104 (2020).
[27]E. Antipov, L. Lykova, and L. Kovba, Koord. Khim. **16**, 770 (1990).
[28]P. Vogt *et al.*, APL Mater. **9**, 031101 (2021).
[29]D. G. Schlom, P. Vogt, F. V. E. Hensling, K. Azizie, Z.-K. Liu, B. J. Bocklund, and S.-L. Shang, "Suboxide molecular beam epitaxy and related structures," U.S. Patent Application No. 0122843 (April 21, 2022).
[30]F. V. Hensling *et al.*, "A high-performance epitaxial transparent oxide thin-film transistor fabricated at back-end-of-line temperature by suboxide molecular-beam epitaxy" (unpublished).
[31]G. Hass, J. Am. Ceram. Soc. **33**, 353 (1950).
[32]M. Fernandez-Perea, M. Vidal-Dasilva, J. I. Larruquert, J. A. Aznarez, J. A. Mendez, E. Gullikson, A. Aquila, and R. Soufli, J. Appl. Phys. **105**, 113505 (2009).

[33]K. M. Adkison, S.-L. Shang, B. J. Bocklund, D. Klimm, D. G. Schlom, and Z.-K. Liu, APL Mater. **8**, 081110 (2020).
[34]J. Sun *et al.*, Phys. Rev. Mater. **6**, 033802 (2022).
[35]G. Koster, G. Rijnders, D. H. A. Blank, and H. Rogalla, Physica C **339**, 215 (2000).
[36]G. Koster, B. L. Kropman, G. J. H. M. Rijnders, D. H. A. Blank, and H. Rogalla, Appl. Phys. Lett. **73**, 2920 (1998).
[37]B. H. Savitzky *et al.*, Ultramicroscopy **191**, 56 (2018).
[38]W. Fischer, Solid State Ionics **116**, 211 (1999).
[39]S. Sasaki, K. Fujino, and Y. Takeuchi, Proc. Jpn. Acad. Ser. B **55**, 43 (1979).
[40]P. N. Arendt and S. R. Foltyn, MRS Bull. **29**, 543 (2004).
[41]C. P. Wang, K. B. Do, M. R. Beasley, T. H. Geballe, and R. H. Hammond, Appl. Phys. Lett. **71**, 2955 (1997).
[42]X. Xiong, S. Kim, K. Zdun, S. Sambandam, A. Rar, K. P. Lenseth, and V. Selvamanickam, IEEE Trans. Appl. Supercond. **19**, 3319 (2009).
[43]J. L. MacManus-Driscoll and S. C. Wimbush, Nat. Rev. Mater. **6**, 587 (2021).
[44]A. Molodyk *et al.*, Sci. Rep. **11**, 1 (2021).
[45]J. H. Haeni, C. D. Theis, D. G. Schlom, W. Tian, X. Q. Pan, H. Chang, I. Takeuchi, and X. D. Xiang, Appl. Phys. Lett. **78**, 3292 (2001).
[46]W. Jesser, Mater. Sci. Eng. **4**, 279 (1969).
[47]E. Machlin and P. Chaudhari, "Synthesis and properties of metastable phases," in *Synthesis and Properties of Metastable Phases*, edited by E. Machlin and T. Rowland (The Metallurgical Society of AIME, Warrendale, 1980), pp. 11–19.
[48]C. P. Flynn, Phys. Rev. Lett. **57**, 599 (1986).
[49]A. Zunger and D. Wood, J. Cryst. Growth **98**, 1 (1989).
[50]A. R. Kaul, O. Y. Gorbenko, and A. A. Kamenev, Russ. Chem. Rev. **73**, 861 (2004).
[51]F. V. Hensling *et al.*, "Is $Ba_3In_2O_6$ a superconductor?" (unpublished).
[52]J. Santiso and M. Burriel, J. Solid State Electrochem. **15**, 985 (2011).
[53]See the supplementary material at https://www.scitation.org/doi/suppl/10.1116/6.0002205 for rocking curves and additional RHEED patterns.
[54]M. R. Barone, M. Jeong, N. Parker, J. Sun, D. A. Tenne, K. Lee, and D. G. Schlom, "Synthesis of metastable Ruddlesden-Popper titanates, $(ATiO_3)_nAO$, with $n \geq 20$ by molecular-beam epitaxy," APL Mater. **10**, 091106 (2022).
[55]F. V. E. Hensling *et al.*, PARADIM data repository, Dataset.